# A Novel CUGexp·MBNL1 Inhibitor with Therapeutic Potential for Myotonic Dystrophy Type 1

Amin Haghighat Jahromi,[†,‡] Lien Nguyen,[‡] Yuan Fu,[‡,⊥] Kali A. Miller,[‡] Anne M. Baranger,[‡,§] and Steven C. Zimmerman*[,‡]

[†]Center for Biophysics and Computational Biology and [‡]Department of Chemistry, University of Illinois, Urbana, Illinois, United States

Ⓢ *Supporting Information*

**ABSTRACT:** Myotonic dystrophy type 1 (DM1) is caused by an expanded CUG repeat (CUGexp) that sequesters muscleblind-like 1 protein (MBNL1), a protein that regulates alternative splicing. CUGexp RNA is a validated drug target for this currently untreatable disease. Herein, we develop a bioactive small molecule (1) that targets CUGexp RNA and is able to inhibit the CUGexp·MBNL1 interaction in cells that model DM1. The core of this small molecule is based on ligand 2, which was previously reported to be active in an *in vitro* assay. A polyamine-derivative side chain was conjugated to this core to make it aqueous-soluble and cell-penetrable. In a DM1 cell model this conjugate was found to disperse CUGexp ribonuclear foci, release MBNL1, and partially reverse the mis-splicing of the insulin receptor pre-mRNA. Direct evidence for ribonuclear foci dispersion by this ligand was obtained in a live DM1 cell model using time-lapse confocal microscopy.
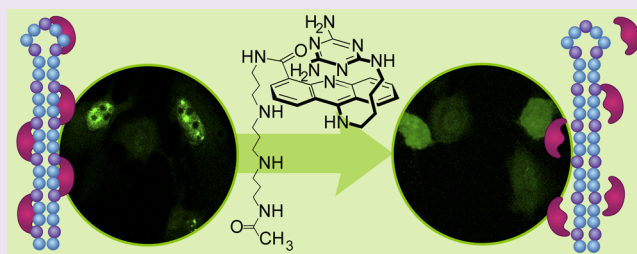
RNA is an important, yet underutilized, drug target. To date, the most common RNA drug targets have been ribosomal RNA and HIV RNA.[1−3] With recent structural and functional discoveries, non-coding RNA is gradually becoming an attractive drug target[4−6] and much is now known about designing ligands to interact with RNA.[7−9] Myotonic dystrophy (dystrophia myotonica, DM) is among the pathologies where RNA stands as the most appropriate target for drug discovery.[10] DM is the most common adult muscular dystrophy with a prevalence of 1:8,000 to 1:20,000 worldwide.[11] Currently there is no treatment for DM, only palliative therapy.[12]

Myotonic dystrophy type 1 (DM1), originates from the progressive expansion of CTG repeats in the 3′-untranslated region of the *DMPK* gene. Thus, expanded CUG repeat transcripts (CUGexp) are the known causative agent of DM1.[13,14] The CUGexp RNA manifests its toxicity through a gain-of-function mechanism involving the sequestration of all three paralogs of human MBNL including MBNL1, a key regulatory protein of alternative splicing.[15−17] The MBNL1·CUGexp aggregate forms ribonuclear foci, a hallmark of DM1 cells.[18] In a mouse model of DM1, a morpholino antisense oligonucleotide (ASO),[19] 2′-*O*-(2-methoxyethyl) ASO,[20] and D-amino acid hexapeptide, each targeting CUGexp, rescued the mis-splicing and reversed the phenotype.[21] These studies validated CUGexp as a drug target and greatly increased interest in finding small molecules that function similarly. Pentamidine,[22] benzo[g]quinolone-based heterocycles,[23] a Hoechst derivative (H1),[24] a modularly assembled Hoechst 33258,[25,26] and ligand 2, reported by our laboratory,[27] are examples of bioactive CUG repeat binders at various stages of development as potential therapeutic agents for DM1.

Our previously reported approach, which led to ligand 2 as a binder of CUG, was based on the notion that selectivity was paramount and could be achieved by rational design focusing on recognition of the UU mismatch in double-stranded CUGexp.[26] We found that the triaminotriazine ring (recognition unit) has a key role in the inhibition of (CUG)$_{12}$·MBNL1 interaction as several acridine derivatives that lacked this unit showed no inhibition potency in an *in vitro* assay (Arambula, J. Ph.D. Thesis, University of Illinois, 2008). Although 2 proved to be among the most selective and effective inhibitors of the (CUG)$_{12}$·MBNL1 interaction, despite its *in vitro* activity it was not active in a cellular model of DM1. Its drugability was limited both because of its low water solubility and its inability to penetrate the cellular membrane. Herein we report further development of this small molecule into an active ligand *in vivo* through its conjugation to a cationic polyamine and the first observation using time-lapse confocal microscopy of foci dispersion in live cells that model DM1.

## ■ RESULTS AND DISCUSSION

Ligand 1 (Figure 1) is a conjugate of the previously reported *in vitro* active ligand 2 (Figure 1) and *N*-[3-({3-[(3-aminopropyl)-amino]propyl}amino)propyl] acetamide side chain. The synthesis scheme of 1 is shown in Supplementary Figure 3. The choice of the side chain was guided by four objectives: (1) increasing its aqueous solubility, (2) increasing its affinity to RNA through electrostatic
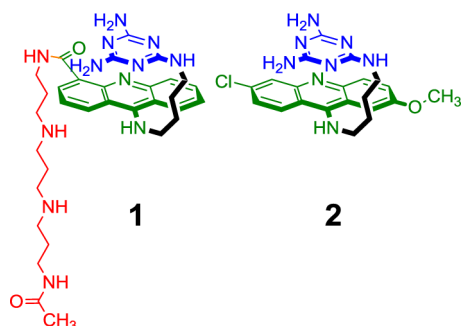
**Figure 1.** Structures of **1** and **2**.

interactions with the phosphate backbone,[28] (3) not adding to its cytotoxicity, and most importantly, (4) making it cell- as well as nucleus-penetrable. In fact, polyamine compounds are essential for cell growth and are easily transported across cellular membranes via the polyamine transporting system (PTS).[29] We were encouraged by the fact that previously reported acridine-polyamine conjugates were recognized by the PTS for cellular uptake.[30,31] These conjugates also exhibited increased activity for nucleic acids.[32]

**Stability of Model CUG^exp and Effect of Ligand 1.** The binding of **1** to a model of CUG^exp was studied by UV melting experiments. Thus, a thermal denaturation study of $(CUG)_{12}$, a validated model of CUG^exp,[33] was carried out in the presence of 1 and 3 equiv of ligand **1** (Figure 2a); simple monophasic melting



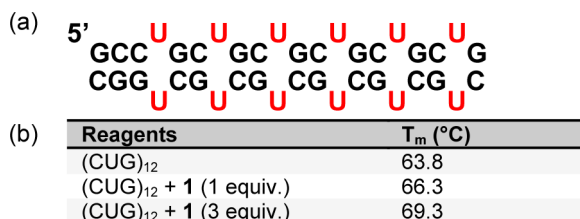**Figure 2.** Ligand **1** stabilizes the ds form of $(CUG)_{12}$. (a) Schematic representation of $(CUG)_{12}$. (b) $T_m$ of $(CUG)_{12}$ hairpin in the presence of 1 and 3 equiv of **1** in 1X PBS buffer. Values were measured in duplicate or triplicate with repeats agreeing within 1%.

curves with a $\Delta T_m$ of 2.5 and 5.5 °C were observed, respectively (Figure 2b and Supplementary Figure 10). This finding indicates binding of **1** to $(CUG)_{12}$ and stabilization of the double-stranded (ds) $(CUG)_{12}$ hairpin. The latter finding is important because it has been proposed that MBNL1 displays a preference for single-stranded (ss) RNA.[34,35] If this model is correct, any ligand that stabilizes the ds form of CUG^exp may prove to be a more effective inhibitor of the $(CUG)_{12}$·MBNL1 interaction. Thus, the observed stabilization of the ds form of $(CUG)_{12}$ was an encouraging result, although not sufficient to ensure selective and effective inhibition of $(CUG)_{12}$·MBNL1 interaction.

**Inhibition of $(CUG)_{12}$·MBNL1 Interaction by 1.** To our knowledge, SPR has not previously been used to characterize the MBNL1·CUG interaction or its inhibition by small molecules.[23,36] Because the technique is particularly well suited for quantifying the binding of proteins to a target on the SPR chip, we developed a simple SPR-based method to directly measure MBNL1 complexation of $(CUG)_{12}$ in real time under equilibrium conditions and in a label-free format. Further, we were able to quantify the inhibition potency of **1** and its selectivity. The selectivity was assessed by performing the assay in the presence of a large excess of competitor tRNA.

Thus, biotinylated $(CUG)_{12}$ was immobilized on a streptavidin-coated SPR sensor chip and incubated with different concentrations of **1** to reach a steady state response (response units, RU, see Figure 3a) over 150 s. The response to the binding of **1** was
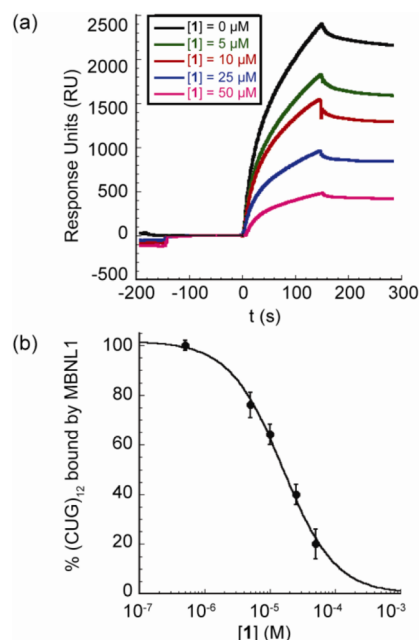


**Figure 3.** Ligand **1** inhibits MBNL1·$(CUG)_{12}$ complex. (a) Representative sensograms from SPR studies. Biotinylated $(CUG)_{12}$ is immobilized on the streptavidin-coated sensor chip. Ligand **1** is injected from $t = -150$ s to $t = 150$ s. GST-MBNL1, 0.65 $\mu$M, is injected from $t = 0$ s to $t = 150$ s. Baseline for the curves was set to RU = 0 at $t = 0$. (b) Fitting data to a dose−response curve indicates inhibition of the $(CUG)_{12}$·MBNL1 interaction in the presence of varying concentrations of **1**. Error bars represent mean ± SD of three replicates.

negligible in comparison to protein binding so the direct contribution of **1** could be ignored. Successive injections of a 0.65 $\mu$M solution of MBNL1 containing the same concentration of **1** as in the preincubation led to varying responses depending on the concentration of **1**. Because the SPR signal directly reflects the binding of MBNL1 to the biotinylated $(CUG)_{12}$, the differences in the response curves are a direct result of inhibition by **1**.

The curves recorded in the presence and absence of 580 $\mu$M yeast tRNA were identical, indicating selective inhibition by **1**. All of the data shown herein were from runs in the presence of tRNA. The maximum RU at 150 s was recorded for each concentration of **1** and converted to the fraction of $(CUG)_{12}$ bound by MBNL1, all values normalized to that measured in the absence of **1**. Fitting the data points in the plot of % $(CUG)_{12}$ bound by MBNL1 versus increasing concentrations of **1** (Figure 3b) gave an apparent $IC_{50}$ value of 15 ± 2 $\mu$M.

These *in vitro* experiments demonstrate that **1** binds to $(CUG)_{12}$, stabilizing the hairpin structure and inhibiting $(CUG)_{12}$·MBNL1 interaction selectively. It is noteworthy that all of the *in vitro* experiments above were carried out with $(CUG)_{12}$ in 1X PBS buffer. This particular buffer was chosen because it is the closest of common buffers to physiological conditions. It is also a more challenging buffer for small molecule inhibitors because it increases the $(CUG)_{12}$·MBNL1 stability, as we obtained a $K_D$ value of 5.2 ± 2.5 nM for $(CUG)_{12}$·MBNL1 interaction in this buffer by SPR technique whereas using EMSA we and others had reported $K_D$ values of 26 and 170 nM, respectively.[27,33]
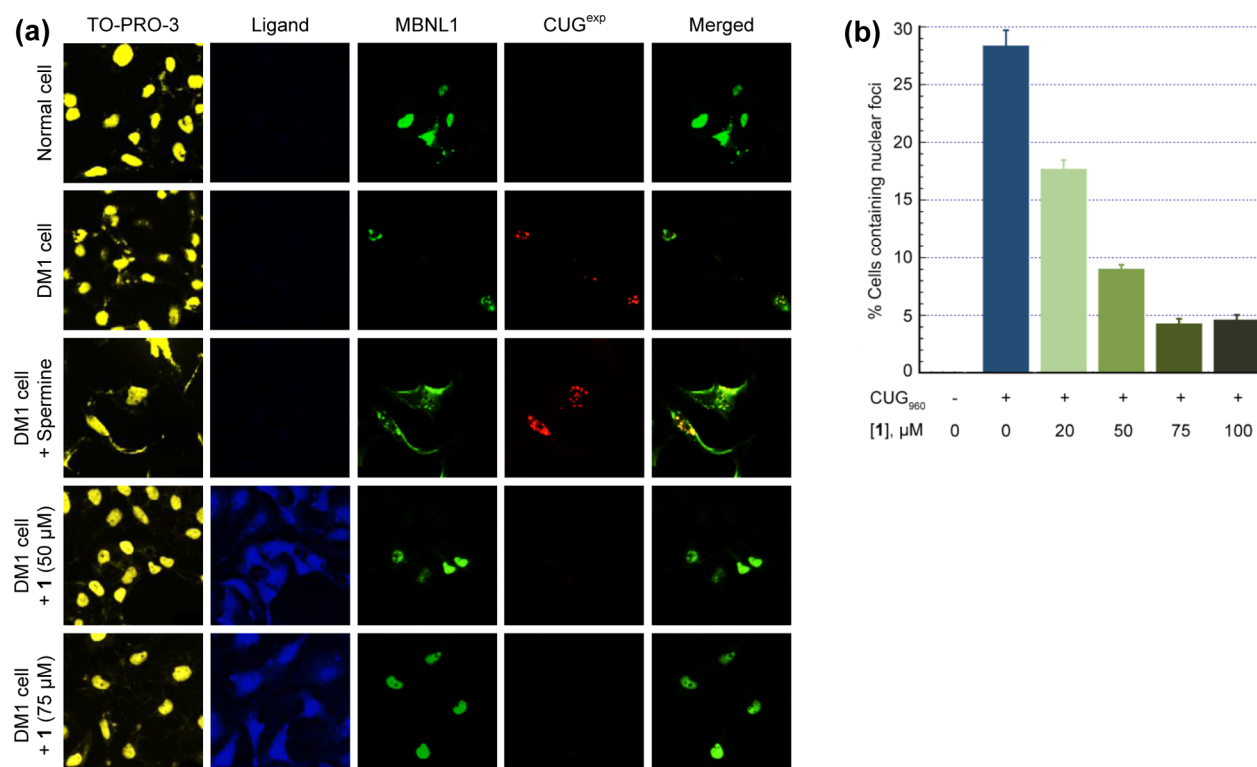
**Figure 4.** Ligand **1** disrupts nuclear foci in fixed DM1 cell model. (a) Columns 1−4 as labeled. Column 5 is merge of columns 3 and 4. Confocal fluorescent images show MBNL1 and CUG$^{exp}$ foci are present in row 2 where no ligand is added as well as row 3 where spermine (50 $\mu$M), as a negative control compound, is added. CUG$^{exp}$ foci are not visible, and MBNL1 is dispersed across the nucleus in negative control cells, row 1, as well as rows 4 and 5 where DM1 cell model is treated with **1** at 50 and 75 $\mu$M, respectively, for 48 h. Each box shows a 150 $\mu$m × 150 $\mu$m area. (b) Plot of CUG$^{exp}$ foci-containing cell fraction at various concentrations of **1**. These data are gathered from scoring over 100 cells. The error bars represent mean ± SE of at least three independent experiments. A magnified CUG$_{960}$ transfected HeLa cell (DM1 cell model) showing ribonuclear foci is shown in Supplementary Figure 12.

**Bioactivity in DM1 Cell Model.** It is a characteristic of DM1 cells that MBNL1 aggregates with CUG$^{exp}$ in nuclear foci.[37] To visualize the effect of **1** on these ribonuclear foci, we used confocal microscopy. This was accomplished using a model for a DM1 cell. Thus, HeLa cells were transfected with two plasmids, truncated DMPK-CUG$_{960}$ and GFP-MBNL1.[38] As a negative control, HeLa cells were transfected with truncated DMPK-CUG$_0$ (i.e., no CUG repeat) and GFP-MBNL1 plasmids.[38] To detect (CUG)$_{960}$ foci, Cy3-(CAG)$_{10}$ was used as a fluorescence *in situ* hybridization (FISH) probe. TO-PRO-3 was used to stain the nucleus; this particular dye was chosen because it has no overlap with the other three fluorophores in our system, i.e., the acridine ring of **1**, the GFP of GFP-MBNL1, and the Cy3 of the FISH probe. By taking advantage of the acridine fluorescence, the penetration of **1** to the cytoplasm as well as nucleus is tracked in the ligand-treated cells.

Representative images from the confocal microscopy are shown in Figure 4. The negative control cells lacking the (CUG)$_{960}$ sequence showed no foci but rather MBNL1 dispersed throughout the nucleus (Figure 4a, row 1). However, co-localized MBNL1 and (CUG)$_{960}$ foci were observed in the DM1 cell model (Figure 4a, row 2). Thus, in the untreated DM1 cells the merged GFP-MBNL1 (green fluorescence) and Cy3-(CAG)$_{10}$ (red fluorescence) images showed yellow spots that correspond to MBNL1 and (CUG)$_{960}$ co-localization in nuclear foci (last column Figure 4). Likewise, incubation of the DM1 cell model with a negative control compound, 50 $\mu$M spermine, for 48 h had no effect on the foci (Figure 4a, row 3). However, incubation with **1**, at 50 and 75 $\mu$M, caused almost complete disappearance of the

(CUG)$_{960}$ foci and dispersion of the MBNL1 fluorescence (Figure 4a, rows 4 and 5, respectively). The foci disruption is observed as a disappearance, rather than dispersion, of the FISH probe, because it is an exogenous antisense nucleic acid probe only visible when concentrated by a highly localized concentration of CUG$^{exp}$ RNA.[39] Cells were classified as having or not having foci. The fraction of cells with (CUG)$_{960}$ foci was reduced by ca. 86% with **1** at 75 $\mu$M with a two-tailed *p*-value of 0.004 (Figure 4b). Similar responses are seen at 50 and 100 $\mu$M ligand.

**Improvement of Pre-mRNA Mis-splicing by 1.** After confirming that **1** disperses the MBNL1 foci, we sought to study the alternative splicing as a downstream measure of recovered MBNL1 regulatory activity. MBNL1 is known to be a key regulatory protein in alternative splicing and affecting many pre-mRNAs, including the insulin receptor (IR).[40] The mis-splicing of IR in DM1 cells occurs with a predominance of isoform A (with exon 11 exclusion) relative to isoform B (with exon 11 inclusion).[41] As described above, truncated DMPK mRNAs containing (CUG)$_{960}$ or no CUG repeats were expressed in HeLa cells to serve as our DM1 cell model and negative control cell, respectively. These cells were co-transfected with an IR mini-gene to study the regulation of splicing of IR by measuring the relative amounts of its two isoforms. Looking at the transcripts in the DM1 cell model showed mis-splicing of IR with 35 ± 2% isoform B (IR-B), whereas 57 ± 1% of IR-B, measured in the negative control cell, was considered the baseline exon inclusion. Treatment of the DM1 cell model with a negative control compound, 50 $\mu$M spermine, had no effect on the IR mis-splicing (Supplementary Figure 9). The splicing assay was

repeated with different concentrations of **1** to see if it was capable of rescuing the mis-splicing of IR, i.e., increasing the fraction of IR-B (Figure 5a).[42] Thus, the DM1 model cells were treated with
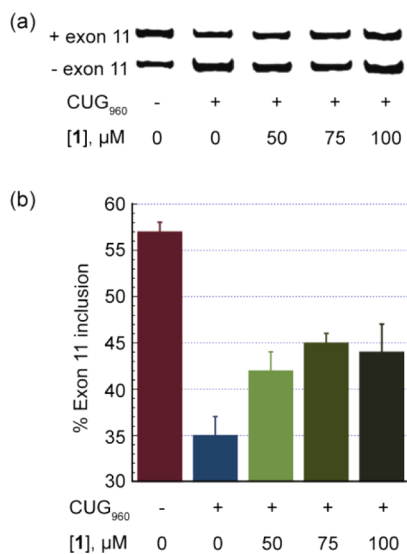


**Figure 5.** Ligand **1** improves mis-splicing of IR in DM1 cell model. (a) Representative gel image of IR alternative splicing. Two bands corresponding to IR isoforms A (+ exon 11) and B (− exon 11), respectively, are derived by reverse transcription-polymerase chain reaction (RT-PCR). DM1 cell model is treated with **1** at 50, 75, and 150 $\mu$M. (b) Plot of the corresponding data shows 40% rescue of mis-splicing at [**1**] = 75 $\mu$M. The error bars represent mean ± SE of 4−6 independent measurements.

**1** at 50, 75, or 150 $\mu$M for 48 h. A rescue of 40% for the IR splicing defect was observed at 75 $\mu$M with 45 ± 1% IR-B measured; two-tailed $p$-values of 0.002 (Figure 5b). Similar responses are seen at 50 and 150 $\mu$M ligand. A more quantitative approach would be needed to demonstrate a dose response. It is noteworthy that cytotoxicity of **1** was evaluated by sulforhodamine B assay and less than 10% HeLa cell death was observed at the highest tested concentration (100 $\mu$M) after 24 h (Supplementary Figure 11).

**MBNL1 Foci Dispersion in Live Cells by 1.** Although the reduction in the foci-containing fixed cells was statistically significant, that experiment represents an indirect measurement of the foci dispersion, because with fixed-cell microscopy, we are not following the same cell directly over time to observe the dispersion of ribonuclear foci upon addition of **1**. Thus, to further confirm our observation, we sought to investigate the effect of **1** in a live cell, by time-lapse confocal microscopy.

To monitor drug uptake and foci dispersion in real time, model DM1 cells were incubated with **1** at 75 $\mu$M, and individual live cells were monitored by confocal microscopy at several time points. The first observation at time point $t = 0$ was made immediately before addition of **1** and MBNL1 nuclear foci were clearly present (Figure 6a, $t = 0$). We found it necessary to use a Petri dish with an imprinted 500 $\mu$m grid to relocate the cell following the incubation interval.

The ability to monitor the location of **1** was made possible by the inherent fluorescence of the acridine unit. Over time, **1** penetrated the cellular and nuclear membrane, and the MBNL1 foci gradually dispersed over the entire nucleus (Figure 6a, $t = 2$, 4, and 7 h). The intensity of a representative MBNL1 focus (the most intense focus) at these four time points shows this

dispersion (Figure 6b). A negative control experiment was performed at the same time points and conditions but without incubation with **1** (Figure 6c). This negative control confirmed the stability of foci over time as the intensity of the GFP-MBNL1 foci was steady (Figure 6d). These results provide direct evidence of the ability of **1** to enter the cell and nucleus and disperse most of the MBNL1·CUG aggregates over a 2−4 h period.

**Conclusion.** Ligand **1** was developed based on a previously reported *in vitro* active ligand.[27] The *in vitro* activity of **1** was assessed by optical melting and surface plasmon resonance (SPR) techniques. Ligand **1** selectively binds to (CUG)$_{12}$, stabilizes its hairpin structure, and inhibits (CUG)$_{12}$·MBNL1 interaction. The polyamine side-chain provides full aqueous solubility that was absent in the initially reported ligand **2**. Ligand **1** penetrates the cellular as well as nuclear membrane. The bioactivity of **1** in model DM1 cells was studied by FISH technique using confocal microscopy and was found to significantly reduce the number of ribonuclear foci. In splicing experiments, **1** partially rescued the IR mis-splicing. Moreover, we studied live DM1 model cells using time-lapse confocal microscopy. For the first time, we were able to observe uptake of a small molecular inhibitor of the (CUG)$_{12}$·MBNL1 interaction by single live cells and further see its ability to disperse the foci over time. This approach is a powerful way to assess directly the effectiveness of small molecules targeted to CUG repeats. The positive results with compound **1** suggest that it is a good candidate for further development and therefore, toxicity and related studies are underway.

## ■ METHODS

**MBNL1N, CUG$_{0/960}$ Plasmid, and RNAs.** The expression vector pGEX-6p-1/MBNL1N was obtained from Maurice S. Swanson (University of Florida, College of Medicine). Wild type DMPK-CUG$_{960}$, DMPK-CUG$_0$ and GFP-MBNL1 mini-genes were obtained from the lab of Thomas Cooper (Baylor College of Medicine). The insulin receptor (IR) mini-gene was obtained from the lab of Nicholas Webster (University of California, San Diego).

The MBNL1 used here is MBNL1N containing the four zinc finger motifs of MBNL1 and a hexa His tag (C-terminus). MBNL1N is known to bind RNA with a similar affinity as the full-length MBNL1 and is commonly used in such studies.[43] All the oligonucleotides were purchased from Integrated DNA Technology and were HPLC purified. The sequences and modifications for RNA constructs used in this study are as follows:

(CUG)$_{12}$ construct for optical melting experiments: 5′−GCCU-GCUGCUGCUGCUGCUGCUGCUGCUGCUGCUGCUGGC−3′

(CUG)$_{12}$ construct for SPR experiments: 5′−GCCUGCUGCUGC-UGCUGCUGCUGCUGCUGCUGCUGCUGGC-TEG-biotin−3′

**MBNL1N Protein Expression and Purification.** Using BL21-CodonPlus(DE3)-RP competent cells (Stratagene), the expression of MBNL1N protein was induced with 1 mM IPTG at OD$_{600}$ 0.6 in LB media with ampicillin for 2 h at 37 °C. Bacterial cells were collected by centrifugation and were then resuspended in a lysis buffer containing 25 mM Tris-Cl (pH = 8), 0.5 M NaCl, 10 mM imidazole, 2 mM BME, 5% glycerol, 0.1% Triton X-100, 2 mg mL$^{-1}$ lysozyme, 0.1 mM PMSF, 1 $\mu$M pepstatin, and 1 $\mu$M leupeptin and sonicated six times for 15 s each. The cell pellet was centrifuged, and the supernatant was collected and filtered through a 45 $\mu$m Millex filter. To purify MBNL1N, Ni-NTA agarose was incubated with the lysate for 1 h at 4 °C and washed with a washing buffer containing 25 mM Tris-Cl (pH = 8), 0.5 M NaCl, 20 mM imidazole, and 0.1% Triton X-100, followed by elution with elution buffer of 25 mM Tris-Cl (pH = 8), 0.5 M NaCl, 250 mM imidazole, and 0.1% Triton X-100. The eluate containing the GST fusion protein was dialyzed against 1X PBS buffer for using in SPR analysis. The molecular weight was confirmed by MALDI mass spectrometry, and the concentration was determined by Bradford assay.
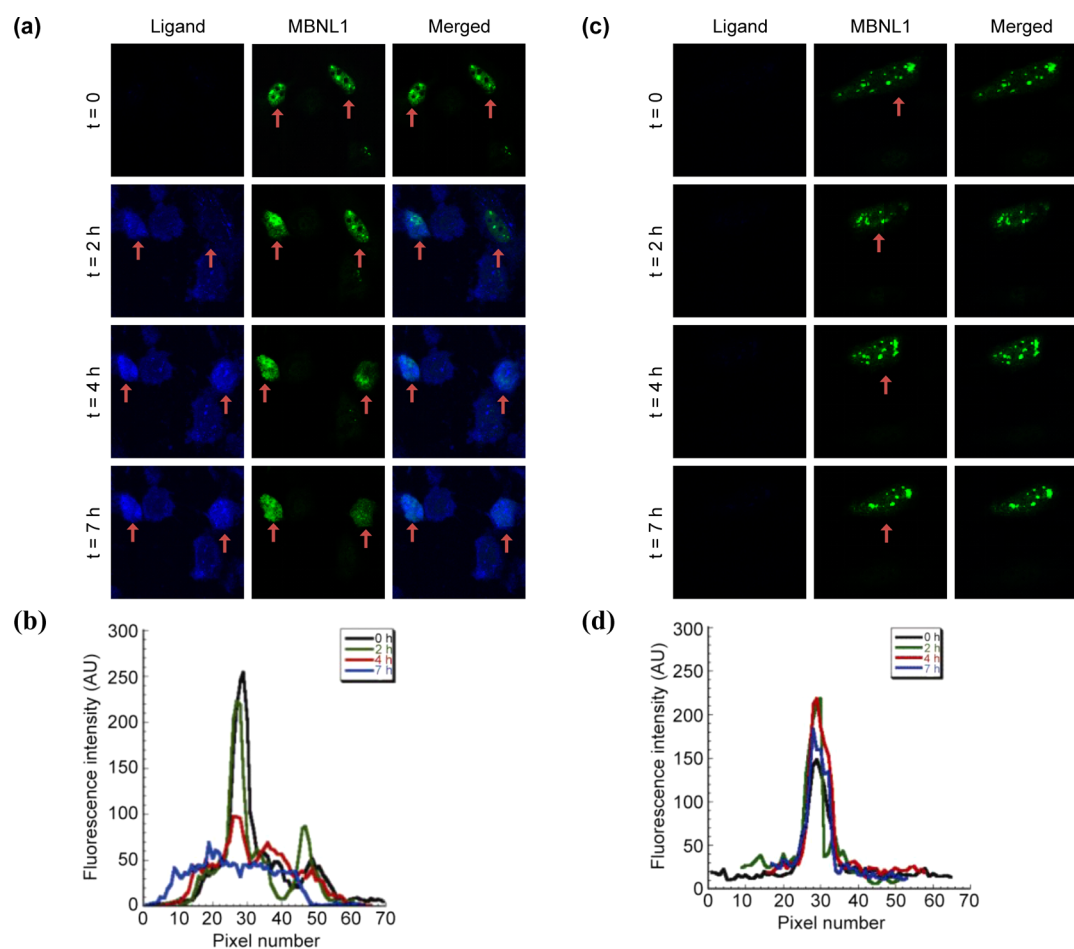
**Figure 6.** Live cell microscopy demonstrates direct evidence for MBNL1 foci dispersion with **1**. (a) Live DM1 model cells are treated with **1** (75 $\mu$M) at $t = 0$, immediately after the first image is taken. Fluoresence of **1** confirms its penetration to the nucleus. MBNL1 nuclear foci are gradually dispersing over time in two cells. Each box shows a 100 $\mu$m × 100 $\mu$m area. (b) Plot of fluorescence intensity of a representative GFP-MBNL1 focus, corresponding to panel a, shows dispersion over time. (c) A single live cell shows stability of foci in a DM1 cell, in the absence of **1**, over the period of 7 h. Each box shows a 100 $\mu$m × 100 $\mu$m area. (d) Plot of fluorescence intensity of a representative GFP-MBNL1 focus, corresponding to panel c, shows no dispersion over time.

**Optical Melting Experiments.** The melting temperature of the $(CUG)_{12}$ was measured on a Shimadzu UV2450 spectrophotometer equipped with a temperature controller. The path length of the cuvettes used was 1 cm. The absorbance of 3.3 $\mu$M $(CUG)_{12}$ in 1X PBS buffer in the absence and presence of 3.3 and 9.9 $\mu$M of **1** was recorded at 260 nm with a slit width of 1 nm from 10 to 95 °C at a ramp rate of 0.5 °C min$^{-1}$. Each profile for melting temperature analysis was generated by subtracting the absorbance of the solution of **1** in 1X PBS buffer from the $(CUG)_{12}$/**1** solution. Melting temperatures were determined by fitting the melting curve using Meltwin 3.5 software.

**Surface Plasmon Resonance (SPR) Analysis.** All SPR experiments were conducted on a streptavidin-coated sensor chip using a Biacore 3000 instrument. Streptavidin-coated research grade sensor chips were preconditioned with three consecutive 1-min injections of 1 M NaCl/50 mM NaOH before the immobilization was started. 3′-Biotin-labeled $(CUG)_{12}$ was captured on flow cell 2 (Response Unit, RU, between 100 and 1100). Flow cell 1 was used as a reference. Inhibition analysis was carried out in PBS 1X buffer, pH = 7.4, containing 0.05% Tween-20 and 0.2 mg mL$^{-1}$ (7.4 or 580 $\mu$M nucleotides) bulk yeast t-RNA to confirm the specificity of inhibition. Various concentrations of **1** were passed over the immobilized RNA at a rate of 20 $\mu$L min$^{-1}$ for 300 s. After the initial 150 s, a solution of GST-MBNL1 protein, 650 nM, in the same buffer was flowed over the surface for 150 s. The reference-subtracted sensograms were obtained by subtracting the measured RU upon injection of PBS buffer from the sensograms. After the dissociation phase, the surface was regenerated,

with a pulse of 0.5% SDS and/or 100 mM NaOH, for a few times followed by a buffer wash to reestablish baseline. For inhibition studies, the resulting sensograms were set to the baseline at $t = 150$ s to offset the binding of **1** to the immobilized $(CUG)_{12}$ surface. The peak RU at $t = 150$ s was recorded and converted to the percentage of $(CUG)_{12}$ bound by MBNL1. All values were normalized to that measured in the absence of **1**. The data points were fit to a four parameter logistic curve to determine the apparent IC$_{50}$ using the following equation by Kaleidagraph software:

$$Y = \frac{Y_{max} - Y_{min}}{1 + \left(\frac{[\mathbf{1}]}{IC_{50}}\right)^n} + Y_{min}$$

where $Y$ is the percentage of $(CUG)_{12}$ bound by MBNL1, $Y_{max}$ and $Y_{min}$ are the maximum and minimum of this percentage, and $n$ is the Hill coefficient. Two or three separate SPR experiments on different sensor chips with different levels of $(CUG)_{12}$ immobilization were carried out to verify that the values are not affected by surface RNA density.

**FISH (Fluorescence *in Situ* Hybridization).** A total of ca. 120,000 HeLa cells were seeded in each well of a 6-well plate on coverslips. After a day, the cells were transfected with 500 ng of DMPK−CUG$_0$ or DMPK−CUG$_{960}$ plasmid and 500 ng of GFP-MBNL1 plasmid using Lipofectamine following the manufacturer's protocol at cell confluence of 70−80%.[38] After 4 h, the media was changed, and **1** was added to each well at different concentrations (20, 50, 75, and 100 $\mu$M). After 2 days, the cells were fixed with 4% PFA and then washed five times with 1X

PBS. Fixed cells were permeabilized with 0.5% triton X-100 in 1X PBS at RT for 5 min. Cells were prewashed with 30% formamide in 2X SSC for 10 min at RT. Cells were probed with FISH probe (1 ng $\mu$L$^{-1}$ of Cy3 CAG$_{10}$ in 30% formamide, 2X SSC, 2 $\mu$g mL$^{-1}$ BSA, 66 $\mu$g mL$^{-1}$ yeast tRNA) for 2 h at 37 °C. Cells were then washed with 30% formamide in 2X SSC for 30 min at 37 °C, followed by washing with 1X SSC for 30 min at RT. The cells were washed twice with 1X PBS, and then nuclei were stained with 1 $\mu$M To-Pro-3 and washed twice. Cells were mounted onto glass sides with ProLong Gold. Slides were imaged at RT by LSM 710, AxioObserver confocal microscopy equipment using a confocal single photon technique with a plan-Apochromat 20x/0.8 M27 objective. Image analysis was performed by Axiovision interactive measurement. The following table indicates the excitation filters used in these experiments.

| fluorophore | component | excitation wavelength (nm) |
| --- | --- | --- |
| acridine | ligand **1** | 405 |
| GFP | MBNL1 | 488 |
| Cy3 | CUG$_{960}$ | 555 |
| TO-PRO-3 | nucleus | 639 |

**IR Splicing Assay.** A total of ca. 120,000 cells were seeded in each well of a 6-well plate in DMEM supplemented with 10% FBS, 4.5 g L$^{-1}$ glucose, L-glutamine, and no antibiotics. After a day, at about 70−80% confluence, the cells were transfected with 500 ng of DMPK−CUG$_0$ or DMPK−CUG$_{960}$ plasmid and 500 ng of IR mini-gene plasmid using Lipofectamine 2000 and Opti-MEM reduced serum medium following the standard protocol.[38,44] The cells were incubated at 37 °C. After 4 h, the transfection medium was replaced by the DMEM medium, and the cells were treated with **1** at three different concentrations (50, 75, and 150 $\mu$M).

After 48 h, cells were harvested, and total RNA was isolated immediately using total RNA isolation kit. Then either the RNA was stored at −80 °C or 1 $\mu$g of the RNA was processed with a reverse transcription step using iScript cDNA synthesis kit. The reverse transcription product was cleaned using Quick Spin kit. Approximately 70 ng of cDNA was used in PCR, 31−35 cycles (within a linear range) using PCR Master Mix kit following the standard protocol. The forward primer was 5′−GTA CCA GCT TGA ATG CTG CTC CT, and the reverse primer was 5′−CTC GAG CGT GGG CAC GCT. PCR products were separated on 8% PAGE gel in 1 X TBE, stained with EtBr in 15 min, destained with water in 15 min, and observed under Molecular Imager.

The gel image was analyzed using ImageJ and the data were plotted using Kaleidagraph. The $p$-values were calculated using two-tailed Student $t$ test.

**Live Cell Imaging.** A total of ca. 120,000 HeLa cells were grown in an Ibidi 35 mm Petri dish with a standard bottom, high walls, and an imprinted 500 $\mu$m relocation grid. After 1 day, cell confluence reached to about 70−80%, and cells were tranfected with 500 ng of DMPK−CUG$_{960}$ plasmid and 500 ng of GFP-MBNL1 plasmid using Lipofectamine following standard protocol. After 4 h, media were changed, and cells were incubated at 37 °C, 5% CO$_2$. Twenty-four hours post-transfection, ligand **1** was added to final concentration of 75 $\mu$M. Live-cell, time-lapse images were taken before addition of **1** as well as at 2, 4, and 7 h time points at RT by a LSM 710, AxioObserver confocal microscopy equipment using a confocal single photon technique with a plan-Apochromat 20x/0.8 M27 objective. Image analysis was performed by Axiovision interactive measurement. For tracking the cells, DIC images were acquired simultaneously with the reflected light images using a TPMT module after setting the Köhler illumination with a fully opened condenser aperture (0.55 NA).

## ■ ASSOCIATED CONTENT

### Ⓢ Supporting Information

Experimental procedures, full characterization data for the compounds, supplementary confocal microscopy and gel images, RNA melting curves and cytotoxicity data. This material is available free of charge via the Internet at http://pubs.acs.org.

## ■ AUTHOR INFORMATION

### Corresponding Author
*E-mail: sczimmer@illinois.edu.

### Present Addresses
§University of California, Berkeley.
⊥Cornell University.

### Notes
The authors declare no competing financial interest.

## ■ REFERENCES

(1) Wilson, W. D., and Li, K. (2000) Targeting RNA with small molecules. *Curr. Med. Chem.* 7, 73−98.

(2) Pearson, N. D., and Prescott, C. D. (1997) RNA as a drug target. *Chem. Biol.* 4, 409−414.

(3) Tor, Y. (2003) Targeting RNA with small molecules. *ChemBioChem* 4, 998−1007.

(4) Guan, L., and Disney, M. D. (2012) Recent advances in developing small molecules targeting RNA. *ACS Chem. Biol.* 7, 73−86.

(5) Thomas, J. R., and Hergenrother, P. J. (2008) Targeting RNA with small molecules. *Chem. Rev.* 108, 1171−1224.

(6) Gallego, J., and Varani, G. (2001) Targeting RNA with small-molecule drugs: therapeutic promise and chemical challenges. *Acc. Chem. Res.* 34, 836−843.

(7) Fulle, S., and Gohlke, H. (2010) Molecular recognition of RNA: challenges for modelling interactions and plasticity. *J. Mol. Recognition* 23, 220−231.

(8) Chow, C. S., and Bogdan, F. M. (1997) A Structural Basis for RNAminus signLigand Interactions. *Chem. Rev.* 97, 1489−1514.

(9) Carlson, C. B., Stephens, O. M., and Beal, P. A. (2003) Recognition of double-stranded RNA by proteins and small molecules. *Biopolymers* 70, 86−102.

(10) Cooper, T. A., Wan, L., and Dreyfuss, G. (2009) RNA and disease. *Cell* 136, 777−793.

(11) Cooper, T. A. (2006) A reversal of misfortune for myotonic dystrophy? *New Engl. J. Med.* 355, 1825−1827.

(12) Foff, E. P., and Mahadevan, M. S. (2011) Therapeutics development in myotonic dystrophy type 1. *Muscle Nerve* 44, 160−169.

(13) Gomes-Pereira, M., Cooper, T. A., and Gourdon, G. (2011) Myotonic dystrophy mouse models: towards rational therapy development. *Trends Mol. Med.* 17, 506−517.

(14) Mirkin, S. M. (2007) Expandable DNA repeats and human disease. *Nature* 447, 932−940.

(15) O'Rourke, J. R., and Swanson, M. S. (2009) Mechanisms of RNA-mediated disease. *J. Biol. Chem.* 284, 7419−7423.

(16) Kanadia, R. N., Shin, J., Yuan, Y., Beattie, S. G., Wheeler, T. M., Thornton, C. A., and Swanson, M. S. (2006) Reversal of RNA missplicing and myotonia after muscleblind overexpression in a mouse poly(CUG) model for myotonic dystrophy. *Proc. Natl. Acad. Sci. U.S.A.* 103, 11748−11753.

(17) Grammatikakis, I., Goo, Y. H., Echeverria, G. V., and Cooper, T. A. (2011) Identification of MBNL1 and MBNL3 domains required for splicing activation and repression. *Nucleic Acids Res.* 39, 2769−2780.

(18) Wheeler, T. M., Krym, M. C., and Thornton, C. A. (2007) Ribonuclear foci at the neuromuscular junction in myotonic dystrophy type 1. *Neuromuscular Disord.* 17, 242−247.

(19) Wheeler, T. M., Sobczak, K., Lueck, J. D., Osborne, R. J., Lin, X., Dirksen, R. T., and Thornton, C. A. (2009) Reversal of RNA dominance

by displacement of protein sequestered on triplet repeat RNA. *Science* **325**, 336−339.

(20) Wheeler, T. M., Leger, A. J., Pandey, S. K., MacLeod, A. R., Nakamori, M., Cheng, S. H., Wentworth, B. M., Bennett, C. F., and Thornton, C. A. (2012) Targeting nuclear RNA for in vivo correction of myotonic dystrophy. *Nature* **488**, 111−115.

(21) Garcia-Lopez, A., Llamusi, B., Orzaez, M., Perez-Paya, E., and Artero, R. D. (2011) In vivo discovery of a peptide that prevents CUG-RNA hairpin formation and reverses RNA toxicity in myotonic dystrophy models. *Proc. Natl. Acad. Sci. U.S.A.* **108**, 11866−11871.

(22) Warf, M. B., Nakamori, M., Matthys, C. M., Thornton, C. A., and Berglund, J. A. (2009) Pentamidine reverses the splicing defects associated with myotonic dystrophy. *Proc. Natl. Acad. Sci. U.S.A.* **106**, 18551−18556.

(23) Ofori, L. O., Hoskins, J., Nakamori, M., Thornton, C. A., and Miller, B. L. (2012) From dynamic combinatorial 'hit' to lead: in vitro and in vivo activity of compounds targeting the pathogenic RNAs that cause myotonic dystrophy. *Nucleic Acids Res.* **40**, 6380−6390.

(24) Parkesh, R., Childs-Disney, J. L., Nakamori, M., Kumar, A., Wang, E., Wang, T., Hoskins, J., Tran, T., Housman, D., Thornton, C. A., and Disney, M. D. (2012) Design of a bioactive small molecule that targets the myotonic dystrophy type 1 RNA via an RNA motif-ligand database and chemical similarity searching. *J. Am. Chem. Soc.* **134**, 4731−4742.

(25) Pushechnikov, A., Lee, M. M., Childs-Disney, J. L., Sobczak, K., French, J. M., Thornton, C. A., and Disney, M. D. (2009) Rational design of ligands targeting triplet repeating transcripts that cause RNA dominant disease: application to myotonic muscular dystrophy type 1 and spinocerebellar ataxia type 3. *J. Am. Chem. Soc.* **131**, 9767−9779.

(26) Childs-Disney, J. L., Hoskins, J., Rzuczek, S. G., Thornton, C. A., and Disney, M. D. (2012) Rationally designed small molecules targeting the RNA that causes myotonic dystrophy type 1 are potently bioactive. *ACS Chem. Biol.* **7**, 856−862.

(27) Arambula, J. F., Ramisetty, S. R., Baranger, A. M., and Zimmerman, S. C. (2009) A simple ligand that selectively targets CUG trinucleotide repeats and inhibits MBNL protein binding. *Proc. Natl. Acad. Sci. U.S.A.* **106**, 16068−16073.

(28) Fischer, W., Brissault, B., Prevost, S., Kopaczynska, M., Andreou, I., Janosch, A., Gradzielski, M., and Haag, R. (2010) Synthesis of linear polyamines with different amine spacings and their ability to form dsDNA/siRNA complexes suitable for transfection. *Macromol. Biosci.* **10**, 1073−1083.

(29) Palmer, A. J., and Wallace, H. M. (2010) The polyamine transport system as a target for anticancer drug development. *Amino Acids* **38**, 415−422.

(30) Delcros, J. G., Tomasi, S., Carrington, S., Martin, B., Renault, J., Blagbrough, I. S., and Uriac, P. (2002) Effect of spermine conjugation on the cytotoxicity and cellular transport of acridine. *J. Med. Chem.* **45**, 5098−5111.

(31) Sanchez-Carrasco, S., Delcros, J. G., Moya-Garcia, A. A., Sanchez-Jimenez, F., and Ramirez, F. J. (2008) Study by optical spectroscopy and molecular dynamics of the interaction of acridine-spermine conjugate with DNA. *Biophys. Chem.* **133**, 54−65.

(32) Perez-Flores, L., Ruiz-Chica, A. J., Delcros, J. G., Sanchez-Jimenez, F. M., and Ramirez, F. J. (2008) Effect of spermine conjugation on the interaction of acridine with alternating purine-pyrimidine oligodeoxyribonucleotides studied by CD, fluorescence and absorption spectroscopies. *Spectrochim Acta A Mol Biomol Spectrosc* **69**, 1089−1096.

(33) Warf, M. B., and Berglund, J. A. (2007) MBNL binds similar RNA structures in the CUG repeats of myotonic dystrophy and its pre-mRNA substrate cardiac troponin T. *RNA* **13**, 2238−2251.

(34) Fu, Y., Ramisetty, S. R., Hussain, N., and Baranger, A. M. (2012) MBNL1-RNA recognition: contributions of MBNL1 sequence and RNA conformation. *ChemBioChem* **13**, 112−119.

(35) Laurent, F. X., Sureau, A., Klein, A. F., Trous1ard, F., Gasnier, E., Furling, D., and Marie, J. (2012) New function for the RNA helicase p68/DDX5 as a modifier of MBNL1 activity on expanded CUG repeats. *Nucleic Acids Res.* **40**, 3159−3171.

(36) Mann, D. a., Kanai, M., Maly, D. J., and Kiessling, L. L. (1998) Probing Low Affinity and Multivalent Interactions with Surface Plasmon Resonance: Ligands for Concanavalin A. *J. Am. Chem. Soc. 120*, 10575−10582.

(37) Echeverria, G. V., and Cooper, T. A. (2012) RNA-binding proteins in microsatellite expansion disorders: mediators of RNA toxicity. *Brain Res.* **1462**, 100−111.

(38) Ho, T. H., Savkur, R. S., Poulos, M. G., Mancini, M. A., Swanson, M. S., and Cooper, T. A. (2005) Colocalization of muscleblind with RNA foci is separable from mis-regulation of alternative splicing in myotonic dystrophy. *J. Cell Sci.* **118**, 2923−2933.

(39) Long, R. M., Elliott, D. J., Stutz, F., Rosbash, M., and Singer, R. H. (1995) Spatial consequences of defective processing of specific yeast mRNAs revealed by fluorescent in situ hybridization. *RNA* **1**, 1071−1078.

(40) Sen, S., Talukdar, I., Liu, Y., Tam, J., Reddy, S., and Webster, N. J. (2010) Muscleblind-like 1 (Mbnl1) promotes insulin receptor exon 11 inclusion via binding to a downstream evolutionarily conserved intronic enhancer. *J. Biol. Chem.* **285**, 25426−25437.

(41) Savkur, R. S., Philips, A. V., and Cooper, T. A. (2001) Aberrant regulation of insulin receptor alternative splicing is associated with insulin resistance in myotonic dystrophy. *Nat. Genet.* **29**, 40−47.

(42) Kosaki, A., Nelson, J., and Webster, N. J. (1998) Identification of intron and exon sequences involved in alternative splicing of insulin receptor pre-mRNA. *J. Biol. Chem.* **273**, 10331−10337.

(43) Yuan, Y., Compton, S. A., Sobczak, K., Stenberg, M. G., Thornton, C. A., Griffith, J. D., and Swanson, M. S. (2007) Muscleblind-like 1 interacts with RNA hairpins in splicing target and pathogenic RNAs. *Nucleic Acids Res.* **35**, 5474−5486.

(44) Kosaki, A., Nelson, J., and Webster, N. J. (1998) Identification of intron and exon sequences involved in alternative splicing of insulin receptor pre-mRNA. *J. Biol. Chem.* **273**, 10331−10337.